Magnetic Resonance Imaging of Flow-Distributed Oscillations

Melanie M. Britton,*,†,§ Andy J. Sederman,† Annette F. Taylor,‡ Stephen K. Scott,‡ and Lynn F. Gladden†

Magnetic Resonance Research Centre, Department of Chemical Engineering, University of Cambridge, New Museums Site, Pembroke Street, Cambridge, CB2 3RA, United Kingdom, and School of Chemistry, University of Leeds, Leeds, LS2 9JT, United Kingdom

Received: June 8, 2005; In Final Form: July 21, 2005

The formation of stationary concentration patterns in a packed-bed reactor (PBR), using a manganese-catalyzed Belousov−Zhabotinsky (BZ) reaction in a mixed sulfuric−phosphoric acid medium, was studied using magnetic resonance imaging (MRI). The PBR was composed of a column filled with glass beads, which was fed by a continuous stirred tank reactor (CSTR). As the reactor is optically opaque, investigation of the three-dimensional (3D) structure of these reaction−diffusion−advection waves is not possible using conventional image capture techniques. MRI has been used to probe this system and the formation, 3D structure, and development of these waves has been studied. At reactor startup, traveling waves were observed. After this initial period the waves stabilized and became stationary. Once fixed, they were found to be remarkably stable. There was significant heterogeneity of the reaction fronts, which were not flat, as would be expected from a plug-flow reactor. Instead, the reaction wave fronts were observed to be conical in shape due to the local hydrodynamics of the bed and specifically the higher velocities and therefore lower residence times close to the wall of the reactor.

Introduction

The coupling of autocatalytic chemical reaction with flow may provide a robust mechanism for pattern formation in biological systems.[1] Reaction−diffusion−advection models have been suggested in conjunction with gene expression during segmentation,[2] bacterial colonies,[3] marine population dynamics,[4] and contraction patterns observed in the slime mold *Physarum plasmodium*.[5] Biochemical pattern formation observed in spatially resolved flow reactors has also been proposed as a mechanism for stabilization against parasites.[6]

Recently, simple models have predicted that stationary concentration patterns might evolve in a chemical reaction−diffusion−advection system with a constantly forced boundary.[7] The predictions were verified by experiments in which an oscillating chemical reaction was fed into a cylindrical packed-bed reactor (PBR) resulting in flow-distributed oscillations (FDO).[8,9] The stationary concentration patterns correspond to a spatially resolved temporal oscillation and the inflow of fresh chemicals maintains the system far from equilibrium, sustaining the patterns indefinitely. While models reproduce the basic mechanism of chemical band formation, some features remain unexplained, such as increase in pulse intensity with flow rate.[10] The models use a constant flow velocity profile (plug flow), which is assumed to be obtained experimentally by packing the PBR with spherical glass beads. In reality, the fluid flows through the void space along a tortuous path between beads. Wall effects, stagnant pockets, and back flow can all give rise to a significant distribution of flow velocities with typical maximum velocities being around 5 times that of the average velocity.[11] The influence of heterogeneity on the propagation of chemical structures is an important area of research.[12] However, conventional optical imaging techniques are unable to penetrate the interior of the packed-bed reactor. To investigate how the flow characteristics of the reactor affect the structure of the chemical waves, magnetic resonance imaging (MRI) techniques have been used.

MRI has already been demonstrated as a powerful method for reconstruction of chemical reaction−diffusion waves in the liquid phase.[13−16] Image contrast is produced through oscillations in the ratio of the oxidized to reduced form of the metal catalyst, which change the relaxation times of water protons surrounding the catalyst molecules. We demonstrate here that MRI provides a noninvasive means to probe the reaction in a porous medium and analyze three-dimensional (3D) chemical patterns in a reaction−diffusion−advection environment. We examine the structure and stability of stationary chemical patterns in a PBR using the manganese-catalyzed Belousov−Zhabotinsky (BZ) reaction in a mixed sulfuric−phosphoric acid medium. This technique also allows us to simultaneously observe flow-distributed oscillations, the porosity of the medium in which they form, and the flow characteristics of the bed. We demonstrate that the bands, once formed, are conical in shape and remarkably stable despite the nonideal nature of the flow in the reactor.

Experimental Section

Packed Bed Reactor. An outline of the apparatus and procedure are described here; further details can be found elsewhere.[9] Briefly, a cylindrical glass tube of length 1 m and internal diameter 16 mm was packed with soda lime glass beads (1 mm diameter). This was held vertically and fed from the bottom from the outflow of a continuous stirred tank reactor (CSTR) of volume 6 mL containing the Belousov−Zhabotinsky

* Corresponding author. E-mail: m.m.britton@bham.ac.uk.
† University of Cambridge.
‡ University of Leeds.
§ Present address: School of Chemistry, University of Birmingham, Edgbaston, Birmingham, B15 2TT, U.K.

10.1021/jp053063i CCC: $30.25
Published on Web 08/26/2005

(BZ) reaction. Before entering the CSTR the BZ chemicals were separated into two stock solutions so that no reaction occurred until their entry into the CSTR, and the CSTR was operated under steady-state conditions to ensure constant concentrations of species at the boundary (entry) of the packed bed. The flow rate was set using a peristaltic pump, and the average interstitial velocity was determined assuming a porosity of 41% for a consolidated packing of spheres with a column-to-sphere diameter ratio of 16.[17,18]

BZ Reaction. Two stock solutions were prepared using reagent grade chemicals dissolved in a mixture of sulfuric and orthophosphoric acid. Solution A contained malonic acid (MA) and sodium bromide, and solution B contained manganese(II) sulfate and sodium bromate. Initial concentrations in the CSTR were as follows: $[Mn^{2+}]_0 = 6 \times 10^{-4}$ M; $[MA]_0 = 0.15$ M; $[BrO_3^-]_0 = 0.05$ M; $[Br^-]_0 = 0.06$ M; $[H_2SO_4] = 0.6$ M; $[H_3PO_4] = 2.8$ M.

A batch manganese-catalyzed BZ reaction was also performed (with concentrations stated above) and compared with the ferroin-catalyzed BZ reaction (with concentrations $[\text{ferroin}]_0 = 7 \times 10^{-4}$ M, $[MA]_0 = 0.4$ M, $[BrO_3^-]_0 = 0.2$ M, and $[H_2SO_4]_0 = 0.15$ M). Oscillations were monitored using a platinum electrode. It should be noted that the manganese-catalyzed system is extremely sensitive to oxygen and also produces bromine; therefore, the solutions were bubbled with nitrogen and the batch reaction was performed in a sealed container, with no liquid/gas interface, to reproduce the conditions in the CSTR. Experiments in the PBR used degassed solutions and the bed was packed by dropping beads into a tube filled with degassed water, thus avoiding the formation of stagnant pockets. The reactions were performed at ambient temperature (20 °C).

MRI Methods. The NMR spectrometer used was a Bruker DMX-200, with a 4.7 T superconducting magnet, operating at a proton resonance frequency of 200 MHz. All imaging experiments were conducted at room temperature in a 38 mm diameter radio frequency birdcage coil surrounded by a three-axis shielded gradient system with a maximum gradient strength of 20 G cm^{-1} in all three directions. For an introduction to the principles of magnetic resonance (MR) techniques, the reader is referred elsewhere.[19]

Relaxation Time Experiments. Relaxation experiments were performed to measure the spin−lattice, T_1, and spin−spin, T_2, relaxation times of solutions containing oxidized or reduced states of the metal ions. The manganese catalyst is used because imaging using the ferroin catalyst is not possible, due to the formation of ferric ions, which dominate the relaxation times of the surrounding water molecules.[20] A solution of Mn^{2+} ions was produced by dissolving 6×10^{-4} M manganese sulfate in a mixture of 2.8 M H_3PO_4 and 0.6M H_2SO_4. To produce the oxidized solution, 0.05 M BrO_3^- was then added. Inversion recovery experiments[19] were used to measure the T_1 for the two solutions. For each solution 16 experiments were collected with delays between the 180° and 90° pulses logarithmically spaced between 200 μs and 2 s (Mn^{2+}) or 5 s (Mn^{3+}). Carr−Purcell−Meiboom−Gill (CPMG) experiments[19] were used to measure the T_2 for the two solutions. For both solutions 16 experiments were done, where the number of echoes collected ranged from 2 to 256 (Mn^{2+}) or 1024 (Mn^{3+}). In both cases an echo spacing of 3 ms was used, which is comparable with the echo time used in the imaging experiments. At the Mn concentration of 6×10^{-4} M, the T_2 relaxation times for water surrounding the reduced (Mn^{2+}) and oxidized (Mn^{3+}) states were 12 ± 1 ms and 365 ± 5 ms, respectively. The T_1 relaxation times were 107 ± 5 ms (Mn^{2+}) and 410 ± 5 ms (Mn^{3+}).

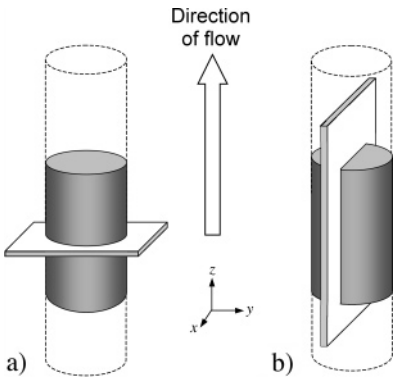

Figure 1. Schematic diagrams indicating field-of-view and image orientation for *xy* slice (a) and *zx* slice (b). In both diagrams the gray area represents the region of the tube held within the radio frequency (rf) coil: the field-of-view.

Imaging Experiments. Images were acquired using the RARE fast imaging technique.[21] This is a robust fast imaging technique and is based on the acquisition of several lines of *k*-space[19] from each excitation, with a refocusing pulse between the acquisition of each line in *k*-space. One of the most important considerations when choosing this imaging sequence is that the image intensities are primarily dependent on T_2, not T_2*, where T_2* is dependent on both the intrinsic T_2 of the system and magnetic field inhomogeneities. This is particularly important in packed beds, where T_2* is typically much less than T_2. Since there will be signal attenuation over the duration of the (T_2-weighted) echo train, signal from protons (^{1}H) with $T_2 \ll$ (echo train duration) will be attenuated and not observed in the image whereas signal from protons with $T_2 \gg$ (echo train duration) will not be significantly attenuated and will appear bright in the image. All radio frequency pulses used in the sequence are slice selective, so multislice images can be acquired; i.e., several parallel images are acquired in the same time that it would normally take to acquire a single image. The orientation of the images is shown in Figure 1.

FDO Experiments. Images were acquired in the *xy* and *zx* planes. The *zx* images were composed of a 256 (vertical) × 128 (horizontal) pixel array with fields-of-view of 45 and 22.5 mm, respectively. Nine vertical slices through the bed of a thickness of 0.8 mm and a separation of 2 mm were taken. The *xy* images were composed of a 128 × 128 pixel array with a field-of-view of 22.5 mm. Horizontal slices, 0.8 mm thick, were acquired for the length of the radio frequency coil at a separation of 2 mm. A RARE factor (the number of echoes acquired per excitation) of 16 was used. The recycle time, between successive excitations in a given imaging plane, was 1.5 s, such that the development of waves was followed by taking multiple images over time, with a time resolution between images of 12 s. The RARE factor of 16 gave an effective echo time, T_{eff}, of 30 ms, resulting in a high signal intensity from the water surrounding Mn^{3+} and virtually no signal from the water surrounding Mn^{2+}.

Traveling Wave Experiments. Images were composed of a 256 (vertical) × 128 (horizontal) pixel array with fields-of-view of 52.4 and 26.2 mm, respectively. A single slice, centered in the middle of the tube, of thickness 2.0 mm was obtained. A RARE factor of 16 was used with a repetition time of 1 s, so the time taken to acquire an image was 8 s. Multiple images were taken with no additional delay between them.

Velocity Imaging Experiments. Velocity imaging experiments of a larger packed bed, also packed with spherical particles, were acquired to show the effect of the ordered structure of the packing close to the walls. This was done in a

larger scale packing to improve the quality and resolution of the velocity images. The images were composed of a 128 × 128 × 128 pixel array with a field-of-view of 47 × 47 × 47 mm. The Reynolds number used in these velocity imaging experiments was the same as those used in the PBR experiments, so the characteristics of the flow here are representative of the flow in the PBR. A consolidated packing of 5 mm ballotini in a 46 mm i.d. column was used in this study. To obtain three velocity components, phase differences in three orthogonal directions were measured, acquiring a total of four 3D images. Detailed discussion of the principles of MRI velocity imaging can be found elsewhere.[19] Experimental details regarding implementation and analysis of 3D images of three velocity components have been reported by Sederman and Gladden.[22]

Results

Stationary chemical patterns have been observed previously in the ferroin-catalyzed BZ reaction in a PBR packed with glass beads.[9] Typical optical images obtained using a CCD camera are shown in Figure 2. In the manganese-catalyzed system visualization of the waves is only possible using MRI experiments because the optical contrast in the packed bed is not sufficient between the oxidized and reduced forms of the catalyst. However, the structure of the bands in both cases is expected to be governed by the form of the temporal oscillations and the effect of flow. For comparison, batch reactions were performed in both the ferroin-catalyzed and manganese-catalyzed BZ reactions. Electrical potential oscillations in the two systems are shown in Figure 3. Both systems display "relaxation" oscillations (i.e., sharp increase followed by slow decrease of the oxidized form of the catalyst) with periods on the order of several minutes. The change in the form of the oscillations in time is due to reactant consumption. This is unlikely to occur in the tubular reactor which is constantly replenished with fresh chemicals and contains no more than five stationary concentration bands.

Zero Flow Reactor Traveling Waves. MR images of traveling (reaction−diffusion) waves in a heterogeneous medium have been acquired by putting the manganese-catalyzed BZ solution into a tube of internal diameter 16 mm, containing 1 mm glass beads. The tube was filled with reactant solution to above the top surface of the glass beads such that convection was not hindered in this bead-free region. By taking vertical (*zx*) images from the center of the tube, the displacement of these waves was observed (Figure 4). The signal comes from the protons within the solvent (water) molecules, so pixels containing beads have no signal. Where there is a predominance of Mn^{2+} ions, the relaxation time of the solvent molecules is very short, so these pixels have low signal intensity and appear dark. Regions where Mn^{3+} predominates appear bright, as a higher signal intensity is detected due to the increased relaxation time of the water molecules. Two main wave sources are observed: one propagating from the bottom of the tube with a long period that results in spherical waves, and one from the bead-free region at the top of the tube with a shorter period that results in planar waves. The solution above the beads shows no stable propagating reaction−diffusion waves principally due to convection. Over the time series of four images, shown at 16 s intervals, the propagation of the waves is observed, most obviously where the waves from the two sources meet and annihilate each other.

Flow-Distributed Oscillations. Flow-distributed oscillations were created in a similarly packed tube by pumping the same reacting mixture to create a PBR. Figure 5 shows a time series of typical images (in the *zx* plane) as the reacting solution is first pumped through the system. Waves of the oxidized form of the catalyst are observed, which appear to propagate from one side of the tube to the other. The traveling waves settle to give stationary concentration bands after a period of approximately 1 h. Figures 6 and 7 show images of a stationary wave taken through the reactor vertically (Figure 6, *zx* plane), and horizontally (Figure 7, *xy* plane). The observable region is 45 mm × 22.5 mm for the vertical images, and 22.5 mm × 22.5 mm for the horizontal images. The volumetric flow rate was 100 $mm^3\ s^{-1}$, producing an interstitial (average) velocity of 1.2 $mm\ s^{-1}$.

Using the series of two-dimensional (2D) images, we were able to reconstruct the three-dimensional structure of the wave. A 3D rendering from the matrix of 2D horizontal slice images (Figure 7) obtained through a stationary wave is shown in Figure 8a. A rotation of the image allows us to clearly see the hollow center of the conelike structure (Figure 8b,c).

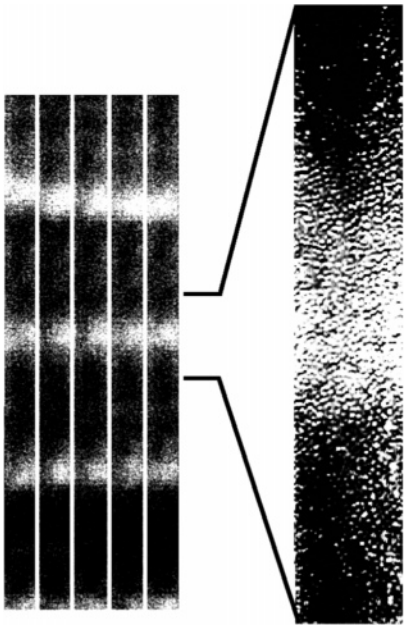

Figure 2. Enhanced optical images (obtained every 10 s) of stationary concentration patterns in the ferroin-catalyzed BZ reaction performed in a tubular PBR of internal diameter 16 mm and packed with 1 mm glass beads. The light region corresponds to the oxidized form of the catalyst. The field-of-view is 500 mm in the five images on the left, and the image on the right shows an enlargement of a single band with a field-of-view of 100 mm. The volumetric flow rate was 200 $mm^3\ s^{-1}$.

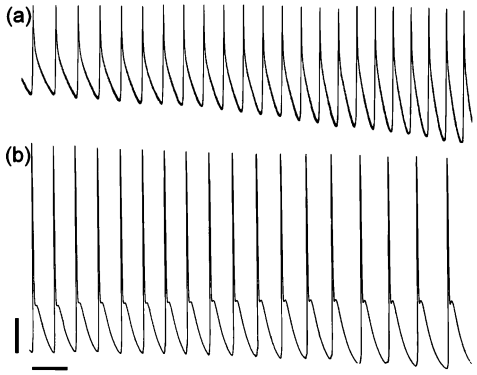

Figure 3. Chart-recorded oscillations in electrical potential during the (a) ferroin-catalyzed BZ reaction and (b) manganese-catalyzed BZ reaction. The vertical bar represents 50 mV, and the horizontal bar represents 5 min.

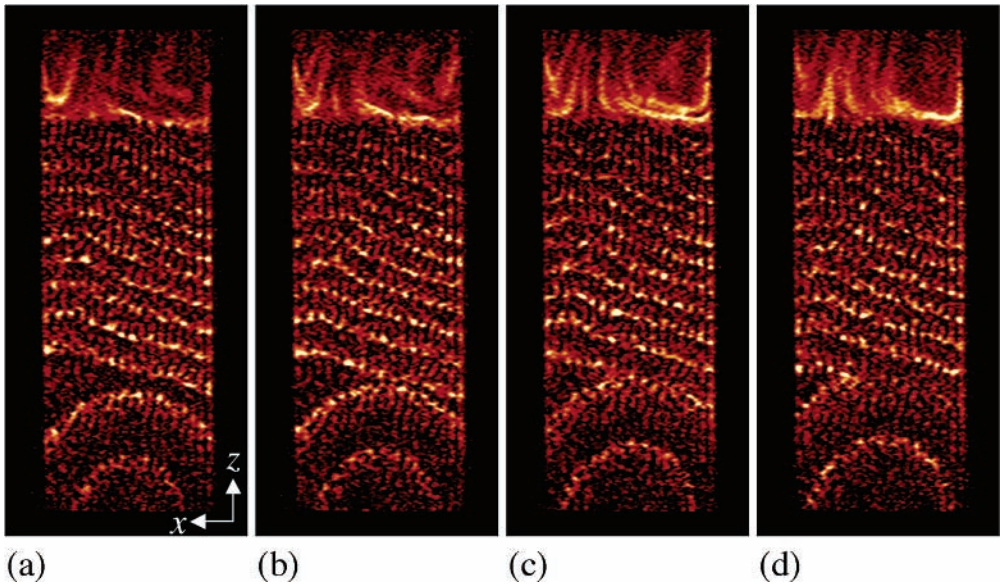

Figure 4. MRI images of traveling (reaction−diffusion) waves in the manganese-catalyzed BZ reaction, taken from the center of the tube. Waves are formed both inside a packed bed of 1 mm glass particles and above in the liquid phase. Images are shown at intervals of 16 s.

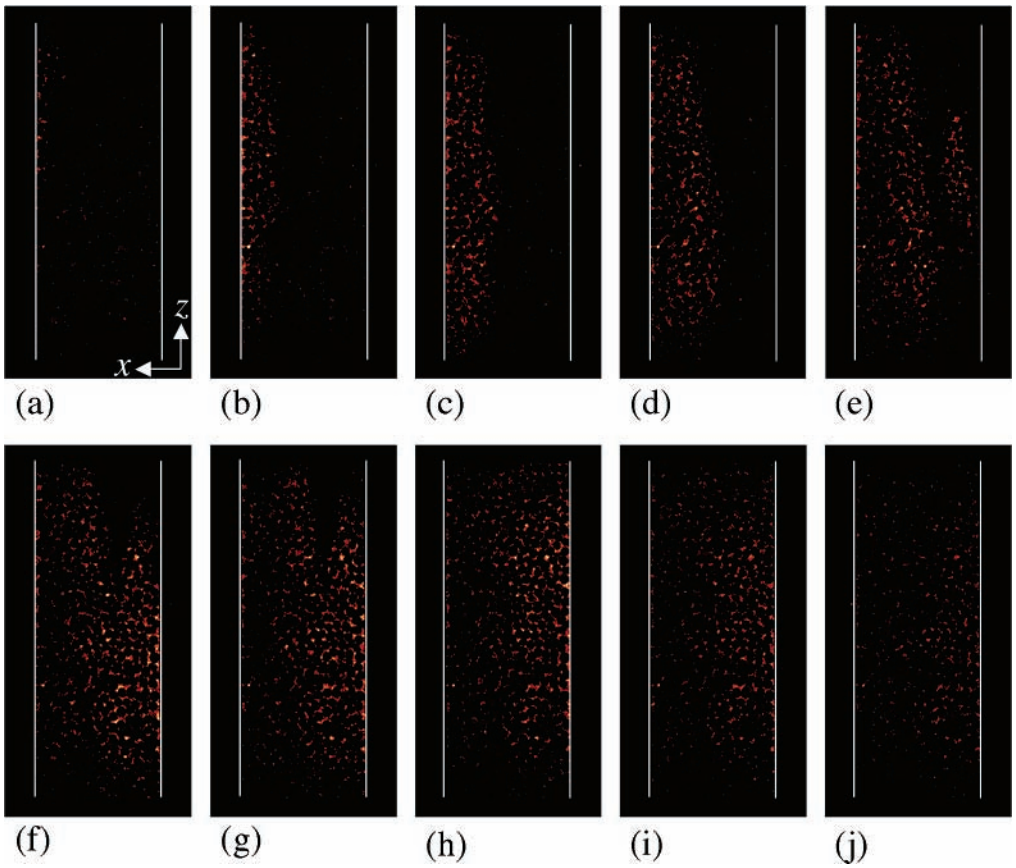

Figure 5. Time series of 10 MRI images of (reaction−diffusion-advection) wave formation as the reactants are first pumped into the packed bed. The images are taken from the center of the tube, with a field-of-view of 45 mm in the vertical direction and 22.5 mm in the horizontal direction and a slice thickness of 0.8 mm. The white lines represent the edge of the glass tube. Images were acquired every 12 s.

Figure 9 shows an image of the bed extending over a vertical distance of 176 mm and shows two wave fronts in the imaging region. This was acquired by moving the reactor bed down and taking successive images over the extent shown in Figure 9. This type of extended image of stationary waves, from which we can accurately measure the wavelength, has been acquired for liquid flow rates of 60 and 100 $mm^3\ s^{-1}$, which correspond to interstitial velocities of 0.7 and 1.2 mm s^{-1}. The stationary patterns at the lower flow rate were achieved by decreasing the flow rate, once the patterns had been established at the higher flow rate. With an interstitial velocity of 1.2 mm s^{-1} the wavelength was determined as 134 ± 10 mm. At an interstitial velocity of 0.7 mm s^{-1} a wavelength of 98 ± 10 mm was determined. We did not investigate the presence of hysteresis, though this is a possibility and should be investigated in future work.

Three-dimensional velocity maps were acquired for a packed bed at a Reynolds number of 1. In Figure 10a a 2D velocity

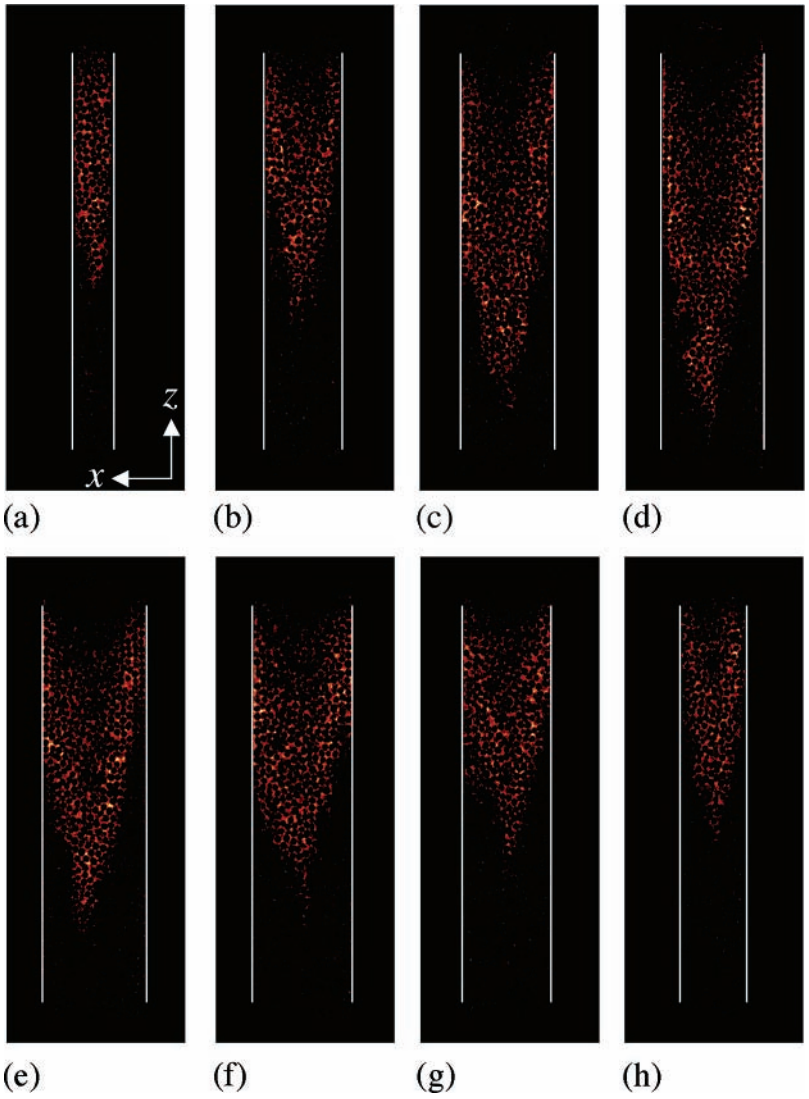

Figure 6. Multiple slice images of a stationary wave taken vertically through the width of the packed bed. The dimensions of the image are the same as Figure 5. The slice thickness of each image is 0.8 mm, with a separation of 2 mm between each image.

image extracted from the 3D data is shown. The gray scale in the void space corresponds to the *z* component (superficial direction) of the local velocity, and glass spheres are shown as black. From this spatially resolved velocity and structural data, radial information can be extracted, and in Figure 10b,c the average velocity and voidage are shown as a function of distance from the reactor wall.

Discussion

The 3D structure of chemical reaction−diffusion waves in liquid phase has been visualized previously using both optical tomography and magnetic resonance imaging (MRI).[14,23] In both cases, the images captured scroll waves of the oxidized form of the catalyst propagating in a homogeneous clear BZ reaction. We use MRI to observe both reaction−diffusion waves and reaction−diffusion−advection waves in a manganese-catalyzed BZ reaction performed in a PBR filled with glass beads.

The addition of glass beads results in a structurally heterogeneous environment, but it reduces convective effects that are known to disrupt pattern formation in the aqueous phase BZ reaction.[13,24,25] In the absence of flow, we observe stable reaction−diffusion waves propagating through the interparticle void space between the glass beads in the cylindrical tube. The resulting pattern is remarkably simple, with waves that extend along the width of the reactor, propagating from the top and the bottom of the tube. Spiral formation is known to occur in spatially heterogeneous excitable media,[26] but we see no evidence of scroll formation in this medium which is indicative of the strong connectivity between channels in this PBR.

When the BZ mixture is pumped through the PBR, the MR images show the development of the expected flow-distributed oscillations.[9] Patterns observed in the ferroin-catalyzed BZ system develop by a "wave-splitting" mechanism, whereby initial bands that formed at some point along the reactor split into two segments, one traveling upstream that settles to form a stationary concentration band, and one traveling downstream that leaves the reactor. This behavior is reproduced by a simple model[27] of the reaction, which assumes plug flow, and is described by the following one-dimensional (1D) reaction−diffusion−advection equations:

$$\frac{\delta u}{\delta t} = D_u \frac{\delta^2 u}{\delta x^2} - \phi \frac{\delta u}{\delta x} + f(u,v) \tag{1}$$

$$\frac{\delta v}{\delta t} = D_v \frac{\delta^2 v}{\delta x^2} - \phi \frac{\delta v}{\delta x} + g(u,v) \tag{2}$$

where u and v represent the concentrations of the autocatalyst

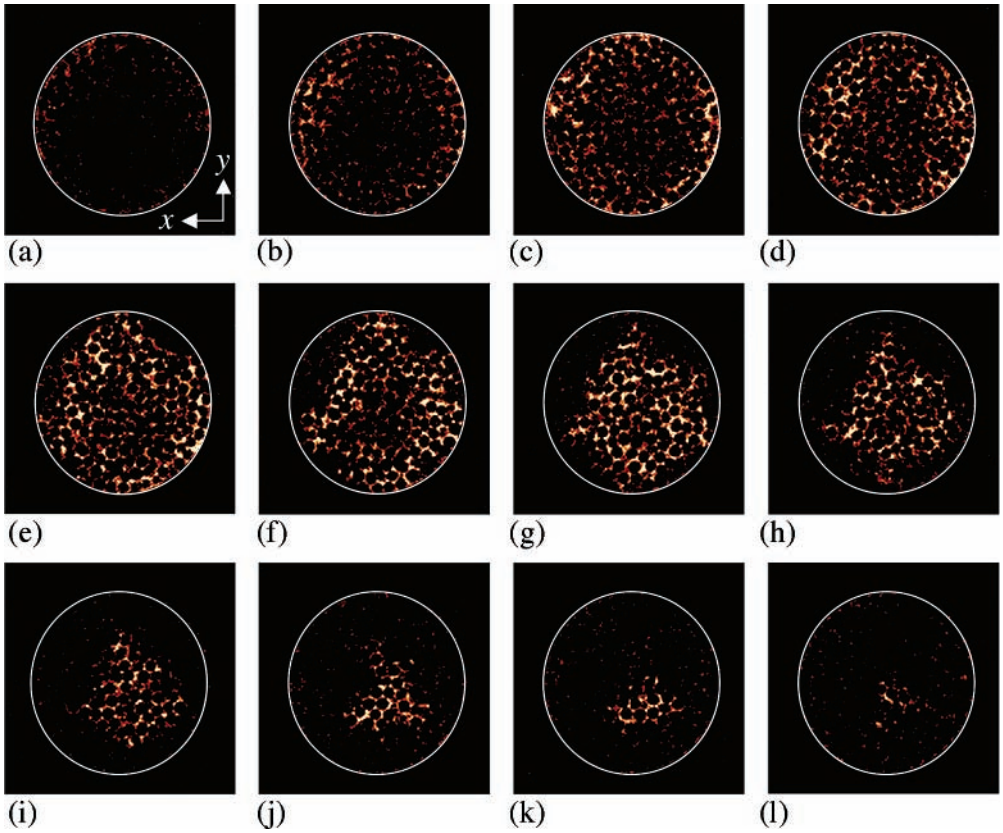

Figure 7. Multiple slice images of a stationary wave taken horizontally through the length of the packed bed. The field-of-view is 22.5 mm in both the *x* and *y* directions, with a slice thickness of 0.8 mm. The separation between each image is 4 mm.

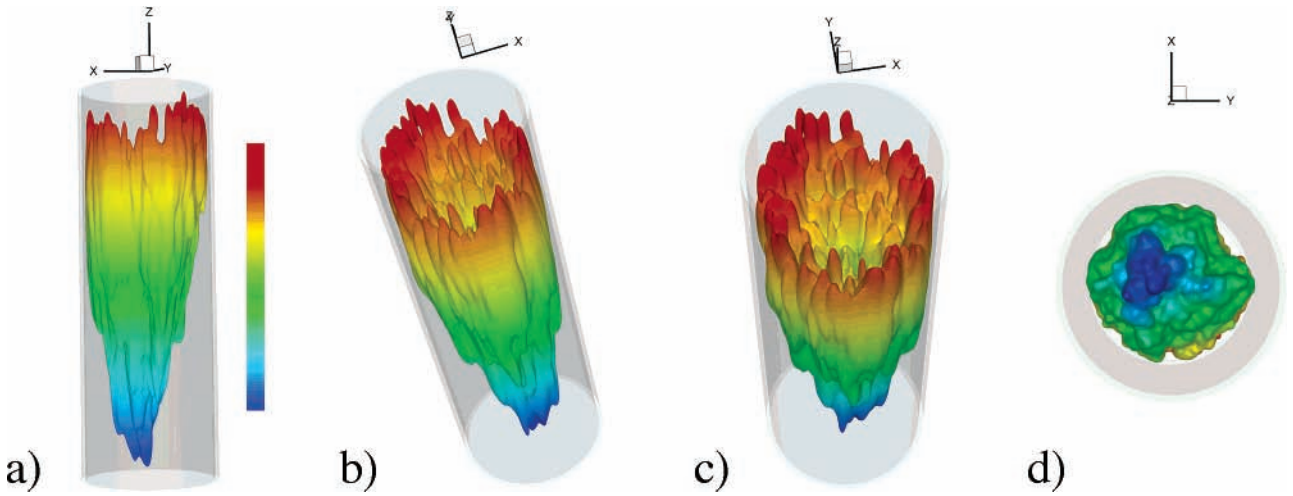

Figure 8. Three-dimensional renderings of a stationary wave in PBR at various orientations. The color scale indicates the height in the bed of fluid in the wave, with blue being upstream and red being downstream. Shading highlights the structure and surface of the wave.

and oxidized form of the metal catalyst, respectively; D_u and D_v are the dispersion (diffusion) coefficients of u and v, respectively; ϕ is the flow rate and $f(u,v)$ and $g(u,v)$ represent chemical reaction terms. The model predicts the existence of a minimum flow velocity of approximately 0.1 mm s^{-1} for stationary waves, depending on the reactant concentrations (in particular the proximity to the Hopf bifurcation). When the flow velocity is slightly greater than the minimum value, the stationary patterns develop in a more complex manner and take longer to settle. In experiments with a particular set of initial concentrations and a flow velocity of 0.9 mm s^{-1}, the stationary patterns were established after an hour, compared to several minutes with a flow velocity of 1.2 mm s^{-1}.[27] Model parameters (for example, certain rate constants) are expected to change upon using manganese as a catalyst, and this may affect the value of the minimum flow velocity. With the flow velocity of 1.2 mm s^{-1} employed in the experiments discussed here, the initial behavior observed by MRI consisted of waves traveling from one side of the tubular reactor to the other. The field-of-view is too small to establish whether these structures corresponded to a wave-splitting event. The fact that the transient behavior lasted an hour suggests that the value of the flow velocity was close to the minimum required for the formation of stationary patterns.

We have obtained the first magnetic resonance (MR) images of chemical patterns in a reaction−diffusion−advection environment and by reconstruction of the images obtained a 3D

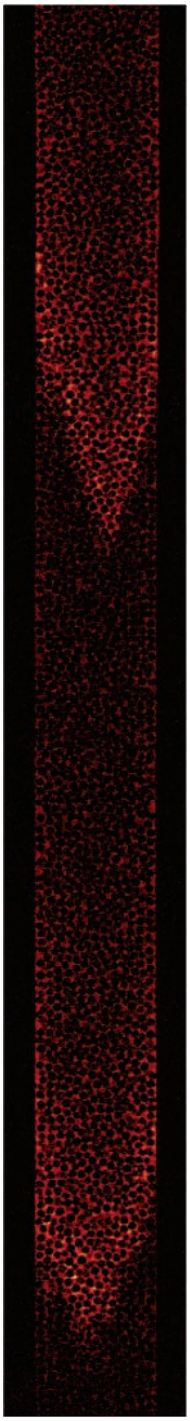

Figure 9. Region of PBR extending over 176 mm showing two stationary wave fronts at a separation of 98 mm at an interstitial velocity of 0.7 mm s^{-1}. This has been produced by acquiring a set of 2D images over a length of the PBR and merging the images together.

image of a single wave of the flow-distributed oscillation. The effect of the additional heterogeneity expected from the distribution of flow velocities in the packed bed is evident in the structure of the stationary wave. From observation of the form of the temporal oscillations, and assuming plug flow, one might expect the concentration band to be planar with a sharp leading edge (upstream) and diffuse tail (downstream). In fact, the stationary pattern is approximately conical in shape, as shown in Figures 6 and 8. Although the wave front is not planar, Figure 9 shows the sharp leading edge followed by the more diffuse tail further along the reactor as the reaction follows the oscillation shown in the electrical potentials in Figure 3. The conical shape means that the same wave front extends over a distance up to 30 mm in the *z* (superficial flow) direction, depending on radial position and local structural and hydrodynamic effects. All wave fronts observed had this broadly conical shape, though the detail of the shape is different for each wave and is determined by more local effects. This approximately conical shape can be explained by consideration of the average local flow rate as a function of radial position. Figure 10b shows that this is a strong function of distance from the wall, with the average flow rate close to the reactor wall being 3 times greater than that in the center of the bed and the average velocity is twice the average velocity in the center of the bed. This variation of the flow is well-known[28,29] and is due to the structural effects imposed by the pseudo-2D packing structure at the wall[17] and leads to a damped oscillation in the voidage away from the wall. The increased velocity close to the wall will correspond to a decrease in the local average residence time, and since the position in the reaction oscillation cycle is strongly influenced by the residence time, this will cause a shift in the reaction front to further along the packing to where the average residence time has increased. Conversely, fluid in the center of the bed has a longer average residence time so that the reaction front moves further upstream, forming the broadly conical shape. If the shape of the reaction front were just due to the local average velocity, and there was no lateral (radial) mixing, the length of the conical front would be much greater and typically the edges would extend up to 3 times the distance into the reactor as the center based on the ratios of local average velocities. This is not the case, and as such, the length of the front is also an indication of the size of the region over which radial mixing is occurring. Although the conical wave front shape often dominates the shape of the interface, many local variations are seen. This can be understood by the distribution of local velocity seen in Figure 10a, where although there are many high-velocity channels close to the wall, there are also several high-velocity channels elsewhere in the bed. These along with the significant stagnant regions observed will cause variations in the local average residence time and therefore in the position of the reaction front, as is observed.

The wavelength of the stationary concentration pattern depends on the flow rate and the natural oscillatory period of the BZ reaction mixture when performed in a batch reactor. The wavelength is also affected by axial dispersion (diffusion), which allows the autocatalytic front to propagate into the unreacted fluid upstream during the wave-splitting development of the stationary pattern. The FDO pattern has an intrinsic period calculated by the product of the wavelength and the inverse flow velocity which, compared to the natural oscillatory period, is a measure of the dispersion in the packed bed. We were able to obtain values of the wavelength at two different flow rates. With a flow velocity of 0.7 mm s^{-1} the wavelength was 98 mm, giving a period of 135 s, and with a flow velocity of 1.2 mm s^{-1} the wavelength was 134 mm, giving a period of 110 s, compared to the natural oscillatory period of 160 s. A decrease in the intrinsic (FDO) period with increasing flow velocity was not evident over the range of operating conditions employed in the experiments of Bamforth et al., but was observed in the experiments and simulations of Kaern and Menzinger,[10] where the value of dispersion coefficient *D* was calculated by the product of the flow velocity and the diameter of the packing in the PBR. The simple 1D model proposed to describe the FDO pattern does not take into account the effect of *radial* dispersion. An increase in radial dispersion would result in increased

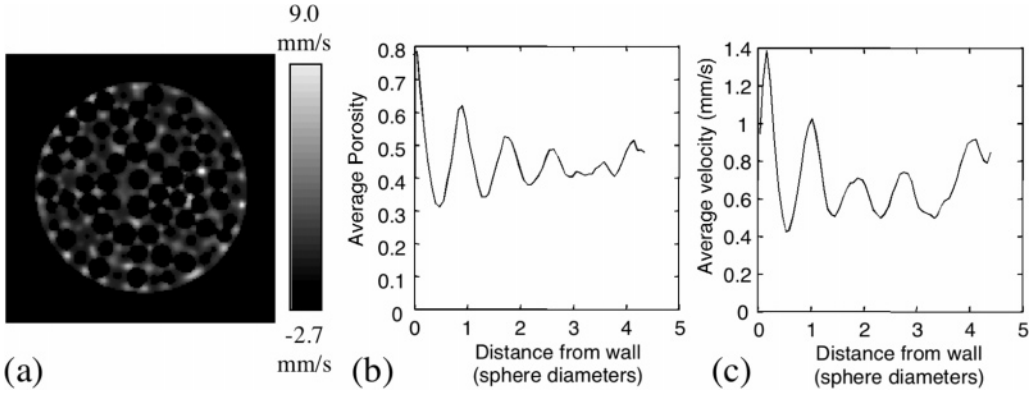

Figure 10. (a) Two-dimensional velocity image, extracted from a 3D data set, of water flowing through an *xy* slice of a PBR. The interstitial velocity was 0.7 mm s^{-1}. The gray scale indicates local *z* velocity, and the beads appear black. (b) Plot of average porosity against distance from wall. (c) Plot of average velocity against distance from wall. Plots b and c have been calculated from the full depth of the 3D velocity image.

coupling laterally and a reduction in the length of the conical front, which may explain the increase in pulse brightness with increasing flow velocity, observed using conventional imaging techniques.[10]

Conclusion

Magnetic resonance imaging provides a means for examining chemical patterns in heterogeneous, optically opaque environments, such as a tubular reactor packed with glass beads. Despite the heterogeneity of the medium in both structure and fluid velocity, self-organization of the oscillating BZ reaction results in simple propagating reaction−diffusion waves and also stationary concentration patterns in a reaction−diffusion−advection environment. NMR imaging techniques have been successfully exploited to produce the first three-dimensional images of stationary chemical structures arising from the interaction between nonlinear chemical reaction, diffusion, and flow. Velocity images in a packing of glass spheres show higher average velocities close to the wall and significant flow heterogeneity elsewhere, which help to explain the conical shape of the reaction front and the nonuniformity of this shape, respectively.

Acknowledgment. M.M.B. thanks the EPSRC for an Advanced Research Fellowship.

References and Notes

(1) Taylor, A. *Adv. Complex Syst.* **2003**, *6*, 155.
(2) Kaern, M.; Menzinger, M.; Hunding, A. *J. Theor. Biol.* **2000**, *207*, 473.
(3) Lega, J.; Passot, T. *Phys. Rev. E* **2003**, *67*, 031906.
(4) Medvinsky, A. B.; Petrovskii, S. V.; Tikhonova, I. A.; Malchow, H.; Li, B. L. *Siam Rev.* **2002**, *44*, 311.
(5) Nakagaki, T.; Yamada, H.; Ito, M. *J. Theor. Biol.* **1999**, *197*, 497.
(6) Kirner, T.; Steen, D.; McCaskill, J. S.; Ackermann, J. *J. Phys. Chem. B* **2002**, *106*, 4525.
(7) Andresen, P.; Bache, M.; Mosekilde, E. *Phys. Rev. E* **1999**, *60*, 297.
(8) Kaern, M.; Menzinger, M. *Phys. Rev. E* **1999**, *60*, R3471.
(9) Bamforth, J. R.; Toth, R.; Gaspar, V.; Scott, S. K. *Phys. Chem. Chem. Phys.* **2002**, *4*, 1299.
(10) Kaern, M.; Menzinger, M. *J. Phys. Chem. B* **2002**, *106*, 3751.
(11) Sederman, A. J.; Johns, M. L.; Alexander, P.; Gladden, L. F. *Chem. Eng. Sci.* **1998**, *53*, 2117.
(12) Xin, J. *Siam Rev.* **2000**, *42*, 161.
(13) Britton, M. M. *J. Phys. Chem. A* **2003**, *107*, 5033.
(14) Cross, A. L.; Armstrong, R. L.; Gobrecht, C.; Paton, M.; Ware, C. *Magn. Reson. Imaging* **1997**, *15*, 719.
(15) Tzalmona, A.; Armstrong, R. L.; Menzinger, M.; Cross, A.; Lemaire, C. *Chem. Phys. Lett.* **1990**, *174*, 199.
(16) Koptyug, I. V.; Lysova, A. A.; Mateev, A. V.; Ilyina, L. Y.; Sagdeev, R. Z.; Parmon, V. N. *Magn. Reson. Imaging* **2003**, *21*, 337.
(17) Benenati, R. F.; Brosilow, C. B. *AIChE J.* **1962**, *8*, 359.
(18) Niu, M.; Akiyama, T.; Takahashi, R.; Yagi, J. *AIChE J.* **1996**, *42*, 1181.
(19) Callaghan, P. T. *Principles of Nuclear Magnetic Resonance Microscopy*; Oxford University Press: Oxford, 1991.
(20) Gao, Y.; Cross, A. R.; Armstrong, R. L. *J. Phys. Chem.* **1996**, *100*, 10159.
(21) Hennig, J.; Naureth, A.; Friedburg, H. *Magn. Reson. Med.* **1986**, *3*, 823.
(22) Sederman, A. J.; Gladden, L. F. *Magn. Reson. Imaging* **2001**, *19*, 565.
(23) Storb, U.; Neto, C. R.; Bar, M.; Muller, S. C. *Phys. Chem. Chem. Phys.* **2003**, *5*, 2344.
(24) Zhang, D. M.; Peltier, W. R.; Armstrong, R. L. *J. Chem. Phys.* **1995**, *103*, 4078.
(25) Zhang, D. M.; Peltier, W. R.; Armstrong, R. L. *J. Chem. Phys.* **1995**, *103*, 4069.
(26) Bub, G.; Shrier, A. *Chaos* **2002**, *12*, 747.
(27) Taylor, A. F.; Bamforth, J. R.; Bardsley, P. *Phys. Chem. Chem. Phys.* **2002**, *4*, 5640.
(28) Schwartz, C. E.; Smith, J. M. *Ind. Eng. Chem.* **1953**, *45*, 1209.
(29) Knox, J. H.; Parcher, J. *Anal. Chem.* **1976**, *41*, 1599.